



Schweizerischer Erdbebendienst  
Service Sismologique Suisse  
Servizio Sismico Svizzero  
Swiss Seismological Service

**ETH**

Eidgenössische Technische Hochschule Zürich  
Swiss Federal Institute of Technology Zurich

# SITE CHARACTERIZATION REPORT

**SNTZ: Naters (VS)**

Francesco Panzera, Manuel Hobiger, Gabriela Gassner-Stamm, Donat Fäh



Last Modification: 5<sup>th</sup> February, 2019

Schweizerischer Erdbebendienst (SED)  
Service Sismologique Suisse  
Servizio Sismico Svizzero  
Servizi da Terratrembels Svizzer

ETH Zürich  
Sonneggstrasse 5  
8092 Zürich  
Schweiz  
[francesco.panzera@sed.ethz.ch](mailto:francesco.panzera@sed.ethz.ch)



# Contents

<b>Contents .....</b>	<b>3</b>
<b>1 Introduction.....</b>	<b>5</b>
<b>2 Geological setting .....</b>	<b>6</b>
<b>3 Site characterization measurements .....</b>	<b>7</b>
<b>3.1 Data set.....</b>	<b>7</b>
<b>3.2 H/V and RayDec ellipticity curves.....</b>	<b>9</b>
<b>3.3 Polarization measurements .....</b>	<b>11</b>
<b>3.4 3-component high-resolution FK.....</b>	<b>11</b>
<b>3.5 WaveDec .....</b>	<b>13</b>
<b>3.6 Summary.....</b>	<b>14</b>
<b>4 Data inversion.....</b>	<b>14</b>
<b>4.1 Inversion targets.....</b>	<b>14</b>
<b>4.2 Inversion parameterization.....</b>	<b>16</b>
<b>4.3 Inversion results .....</b>	<b>16</b>
<b>4.4 Discussion of the inversion result .....</b>	<b>24</b>
<b>5 Further results from the inverted profiles.....</b>	<b>25</b>
<b>5.1 SH transfer function .....</b>	<b>25</b>
<b>5.2 Quarter-wavelength representation .....</b>	<b>26</b>
<b>6 Discussion and conclusions.....</b>	<b>27</b>
<b>References.....</b>	<b>27</b>

## Summary

Naters (VS), on the upper Rhone valley, was selected as site for the installation of a new station, called SNTZ, as part of the renewal project of the Swiss Strong Motion Network (SSMNet). In order to better assess the local underground, we performed site characterization measurements with different techniques. The results of the horizontal-to-vertical spectral ratio (H/V), show curves with clear peaks between 2.0 and 4.0 Hz. This variability is related to a dipping bedrock towards SE underneath the station.

The inversion of the passive seismic array measurements allows to infer three possible discontinuities above the bedrock at 5, 30 and 70 m. The bedrock has a velocity of about 1200 m/s, whereas the shear wave velocity ranges between 200 and 850 m/s above it. The  $V_{S30}$  value of the site is about 418 m/s, corresponding to soil class B in EC8 and C in SIA261.

The theoretical shear-wave transfer functions predict an amplification at about 3.0 Hz, in quite good agreement with the fundamental H/V frequency of the site where the strong motion station is installed.

# 1 Introduction

The station SNTZ is part of the Swiss Strong Motion Network (SSMNet). The station has been installed on 24 October 2017 in the framework of the second phase of the Swiss Strong Motion Network (SSMNet) renewal project (Fig. 1). In order to better characterize the underground of the station, we performed passive array measurements.

The site is of interest because the middle and upper Valais was struck by a strong earthquake on 25 July 1855 that caused damage in a wide area around Visp. In the Earthquake Catalogue of Switzerland (ECOS) (Swiss Seismological Service 2002; Fäh et al., 2003), an epicentral intensity ( $I_0$ ) of VIII and an estimated moment magnitude ( $M_w$ ) of 6.4 are assigned to this event. The epicenter of the earthquake was located about 15 km from Naters and a high percentage of buildings in Naters were damaged grade 3 or 4 in the EMS98 scale (Fritsche et al. 2006). The damage distribution in the Rhone valley suggested that local site effects could have played a role in the emerging damage pattern. For this reason, further extended geophysical and seismological investigations were planned. Such a measurement campaign was carried out on 9 July 2007 in order to characterize the soil column in terms of fundamental frequency and shear wave velocity in Naters. These measurements have been reanalyzed together with an H/V measurement at the location of SNTZ to characterize the underground structure.

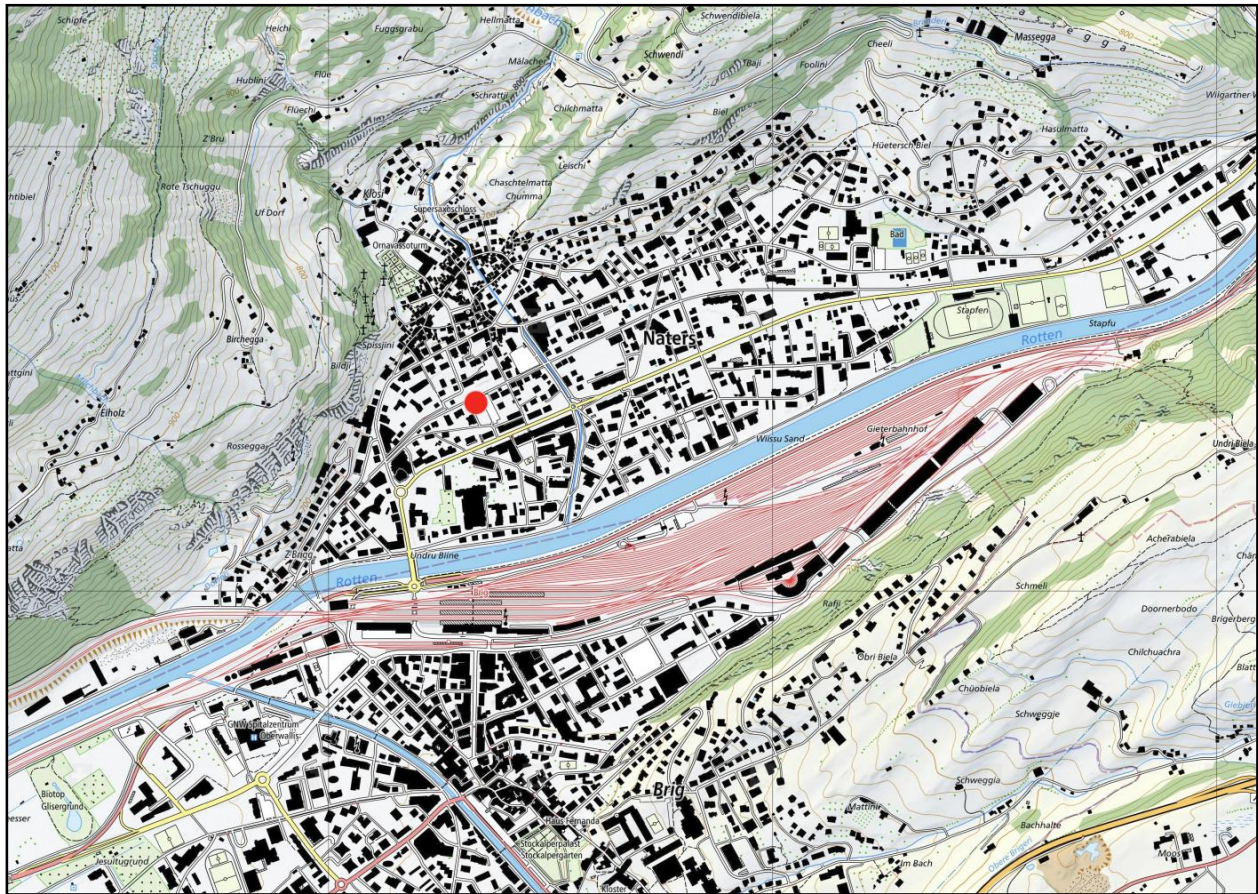
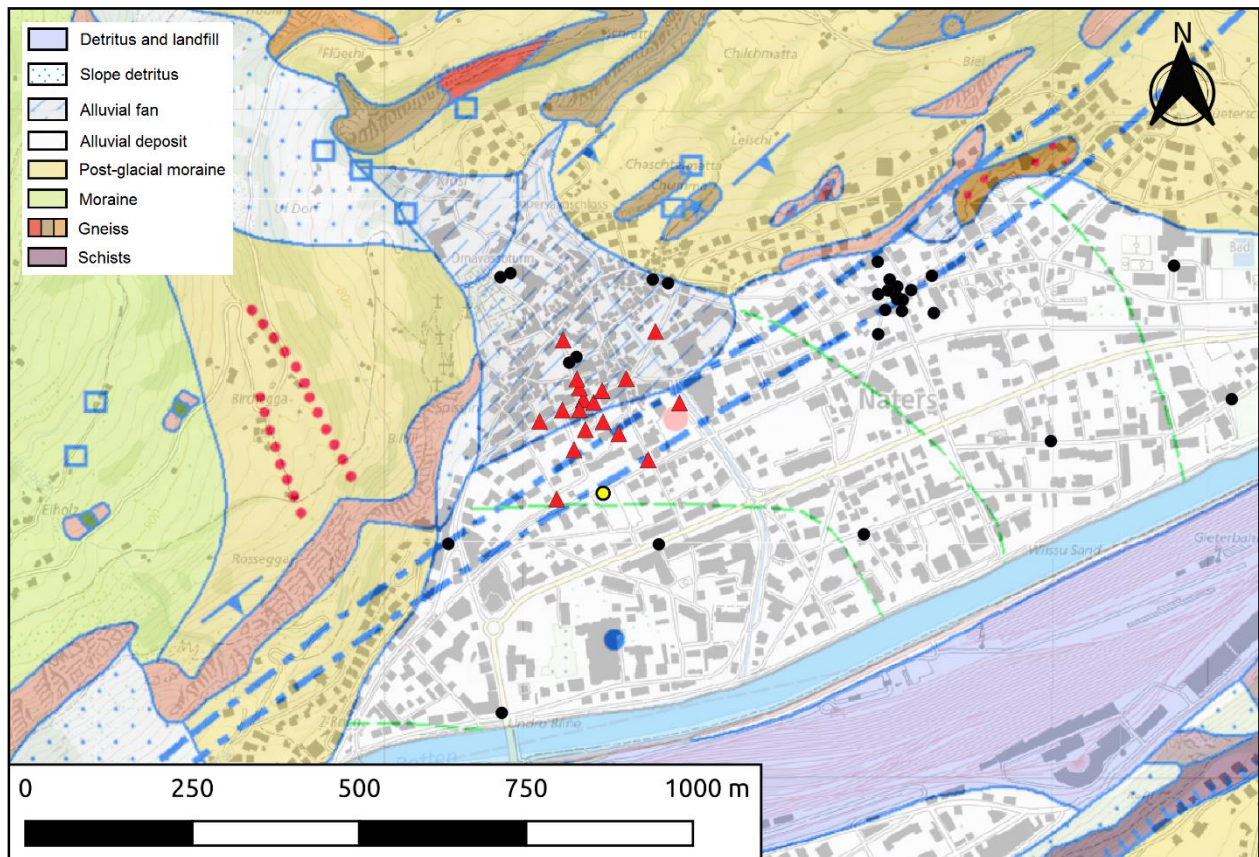


Figure 1: Map showing the location of the strong motion station (red circle) in Naters. © 2019 swisstopo (JD100042)

## 2 Geological setting

A geological map of the surroundings of the site in Naters is shown in Fig. 2, together with the stations of the passive array measurements. Eleven stations of the passive array measurement lie on Quaternary alluvial fans, whereas seven were deployed on alluvial deposits. The seismic station SNTZ is located near the north flank of the upper Rhone valley on the alluvial deposits.



*Figure 2: Geological map of Naters. The stations of the passive array recordings are indicated by red triangles, black dots are available measurements in the area, whereas the SNTZ strong motion station position is showed by a yellow circle.*

## 3 Site characterization measurements

### 3.1 Data set

To characterize the deeper underground structure around the seismic station, we reanalyze the passive seismic measurements performed in 2007, together with a new H/V measurement at the location of SNTZ.

Two array configurations were used, for a total of 4 rings of 12, 30, 75 and 150 m radius around a central station NAT1\_00 (Fig. 3). The innermost ring consisted of three stations, the other rings of five stations each.

The first configuration (configuration A) includes the 3 inner rings (14 sensors in total); the second configuration (configuration B) includes the 2 outer rings and the central station (11 sensors in total). The experimental setup is displayed in Fig. 3. The minimum and maximum interstation distances in the first configuration were 15.0 and 94.0 m, respectively, and in the second configuration 73.0 and 150.0 m.

For the array measurements, 12 Quanterra Q330 dataloggers named NR01 to NR12 and 14 Lennartz 3C 5 s seismometers were used. Each datalogger can record on 2 ports A (channels EH1, EH2, EH3 for Z, N, E directions) and B (channels EH4, EH5, EH6 for Z, N, E directions). Time synchronization was ensured by GPS. The sensors were placed on metal tripods, either in a 10 cm deep hole dug in the ground for better coupling, or directly on asphalt or rock. The array recording time was 57 minutes (3420 s) for the small array and 58 minutes (3480 s) for the larger array configuration. The station locations have been measured by a differential GPS system (Leica Viva GS10) which was set up to measure with a precision better than 5 cm.

We performed an additional H/V measurement next to station SNTZ (Fig. 4) and used other H/V measurements performed in the past (Fig. 3).



Figure 3: Layout of the array measurement in Naters. The locations of the stations for the passive seismic measurement are indicated by the red triangles, the yellow dots indicate additional single-station measurements near SNTZ. In particular, NAT49 was performed at the station site. © 2019 swisstopo (JD100042)



Figure 4: Seismic station installation example for the measurements in Naters.

### 3.2 H/V and RayDec ellipticity curves

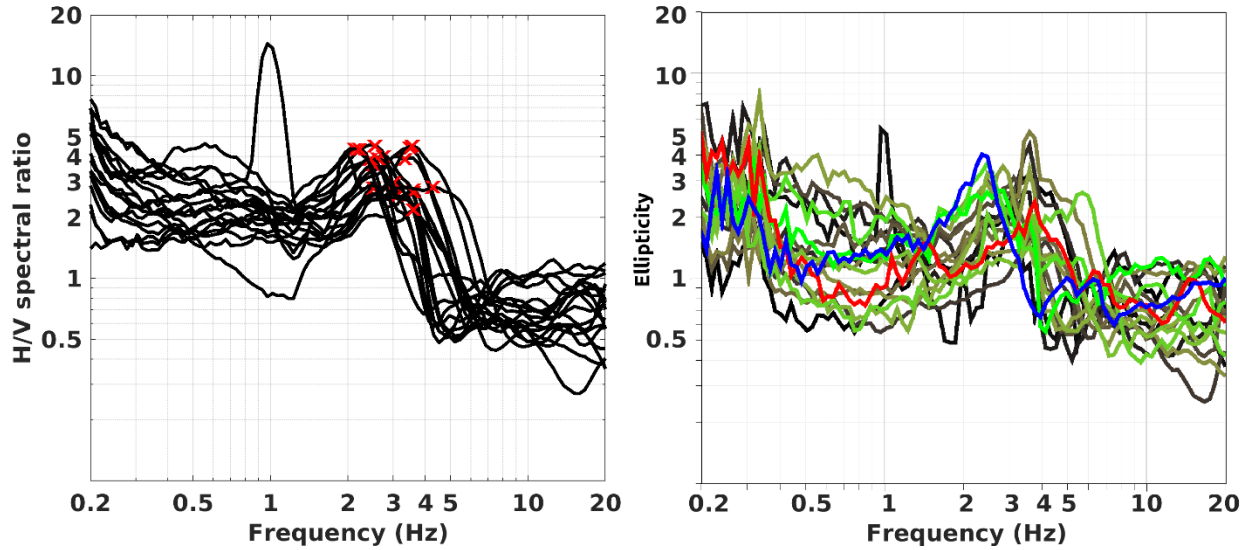


Figure 5: Left: H/V curves of the different stations of the array measurements in Naters. Right: RayDec ellipticities for all stations of the array. The curves of NAT1\_00, the array center, and NAT49, nearby the station site, are highlighted in red and blue, respectively.

Figure 5 shows the H/V curves determined with the time-frequency analysis method (Fäh et al., 2009) for all stations of the passive array. The H/V curves are not homogeneous and show clear peaks between 2.0 and 4.0 Hz. Below 2.0 Hz and above 4.0 Hz, the different curves are more variable. The RayDec technique (Hobiger et al., 2009) is meant to eliminate the contributions of other wave types than Rayleigh waves and give a better estimate of the ellipticity than the classical H/V technique. The RayDec ellipticity curves for all stations of the array measurements are shown in Fig. 5. The RayDec curves of the different stations are also not homogeneous, but show different fundamental peaks.

The peak variability was investigated by plotting map of the fundamental frequencies (Fig. 6) and performing an H/V transect from the northwest to the southeast (Fig. 7; Panzera et al. 2018). From the fundamental frequency map (Fig. 6), it is possible to observe a decrease in frequency towards southeast, which is better highlighted through the H/V 2D profile (Fig. 7). These observations allow us to infer the geometry of the bedrock, which is not horizontal, but seems to slope towards the southeast.

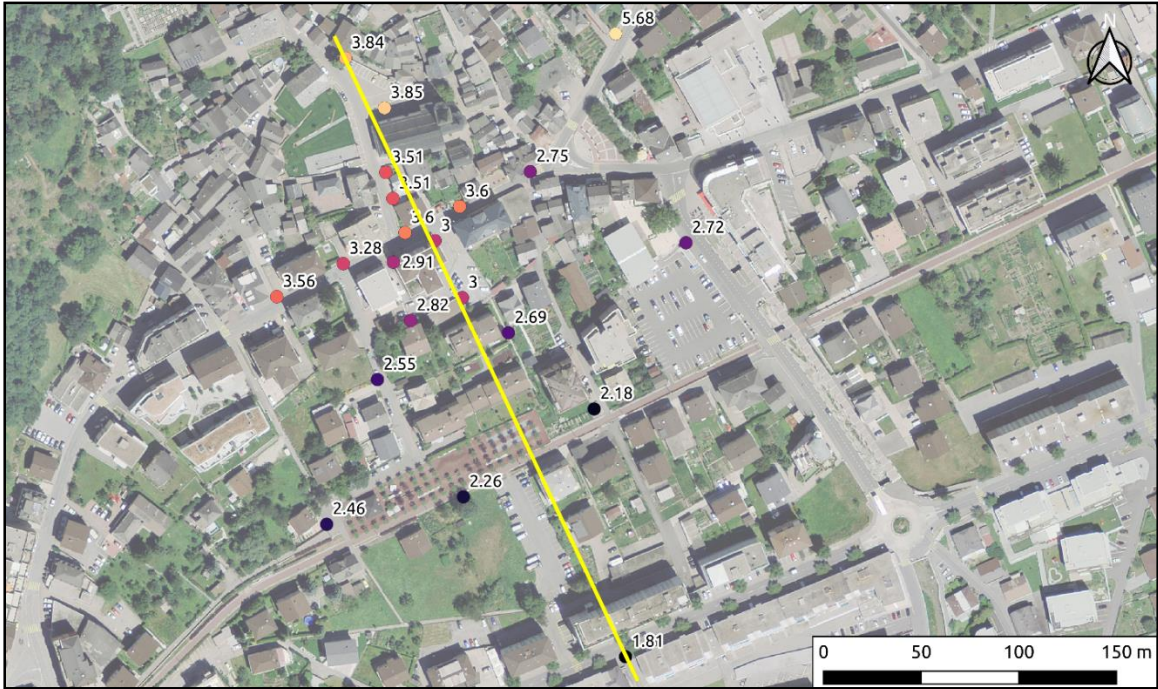


Figure 6: Fundamental frequency map. The yellow line indicates the direction of the H/V profile in Fig. 7.

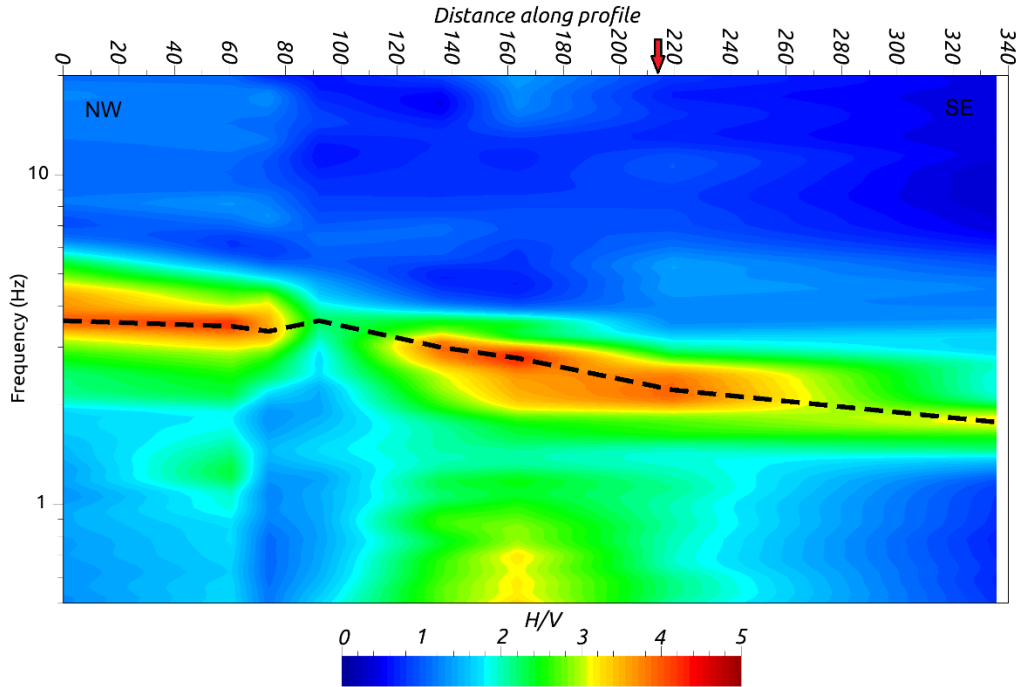


Figure 7: Cross-section obtained by combining the ambient vibration measurements along the transect (yellow line in Fig. 5). The picture is obtained by plotting and interpolating the H/V curves of the different stations along the profile. The red arrow shows the approximate position of SNTZ.

### 3.3 Polarization measurements

The polarization analysis was performed according to Burjánek et al. (2010) and Burjánek et al. (2012). The results for all stations of the array are similar. Only the results for NAT49, next to SNTZ (see location in Fig. 3), are shown in Fig. 8. The results show that the ground motion is almost linear and horizontally polarized around the H/V peak. Two orthogonal polarization directions oriented NW and ENE are visible, with frequencies at about 1.5 and 2.0 Hz, respectively. These polarization directions are not very pronounced but may correspond to a 2D/3D behavior of the alluvial fan and the Rhone valley.

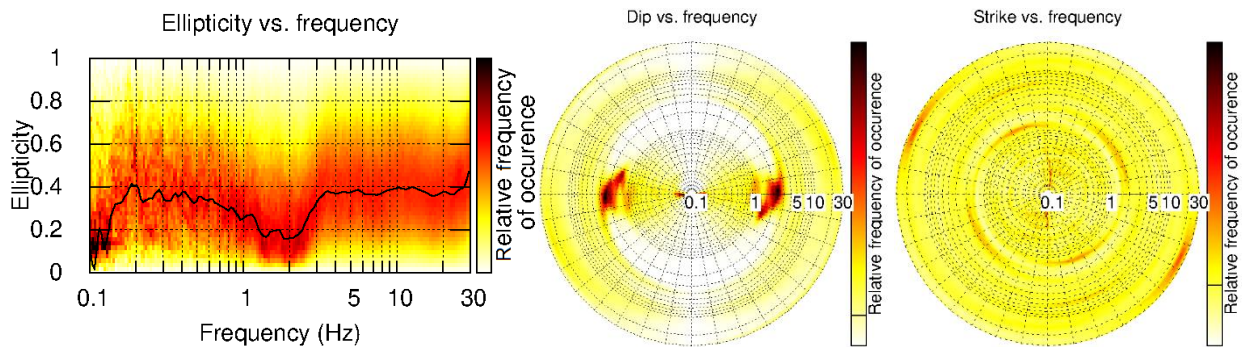


Figure 8: Polarization analysis of station NAT49.

### 3.4 3-component high-resolution FK

The results of the 3-component high-resolution FK analysis (Poggi and Fäh, 2010) are shown in Fig. 9. The analysis was performed for each of the two array configurations independently.

The results on the transverse component for configuration A show the dispersion curve (DC) of the fundamental mode of Love waves from 3.0 to 3.5 Hz and a second branch, possible the fundamental first higher mode, from 3.9 to 9.0 Hz. On the radial component, no dispersion curve is visible. On the vertical component, the fundamental mode can be picked between 3.6 and 14.0 Hz. The corresponding ellipticity curve of the vertical component is clearly identified in the respective frequency range and mostly flat.

The results of configuration B show a dispersion curve on the transverse component between 2.5 and 5.0 Hz. On the radial and vertical components, no dispersion curves are visible.

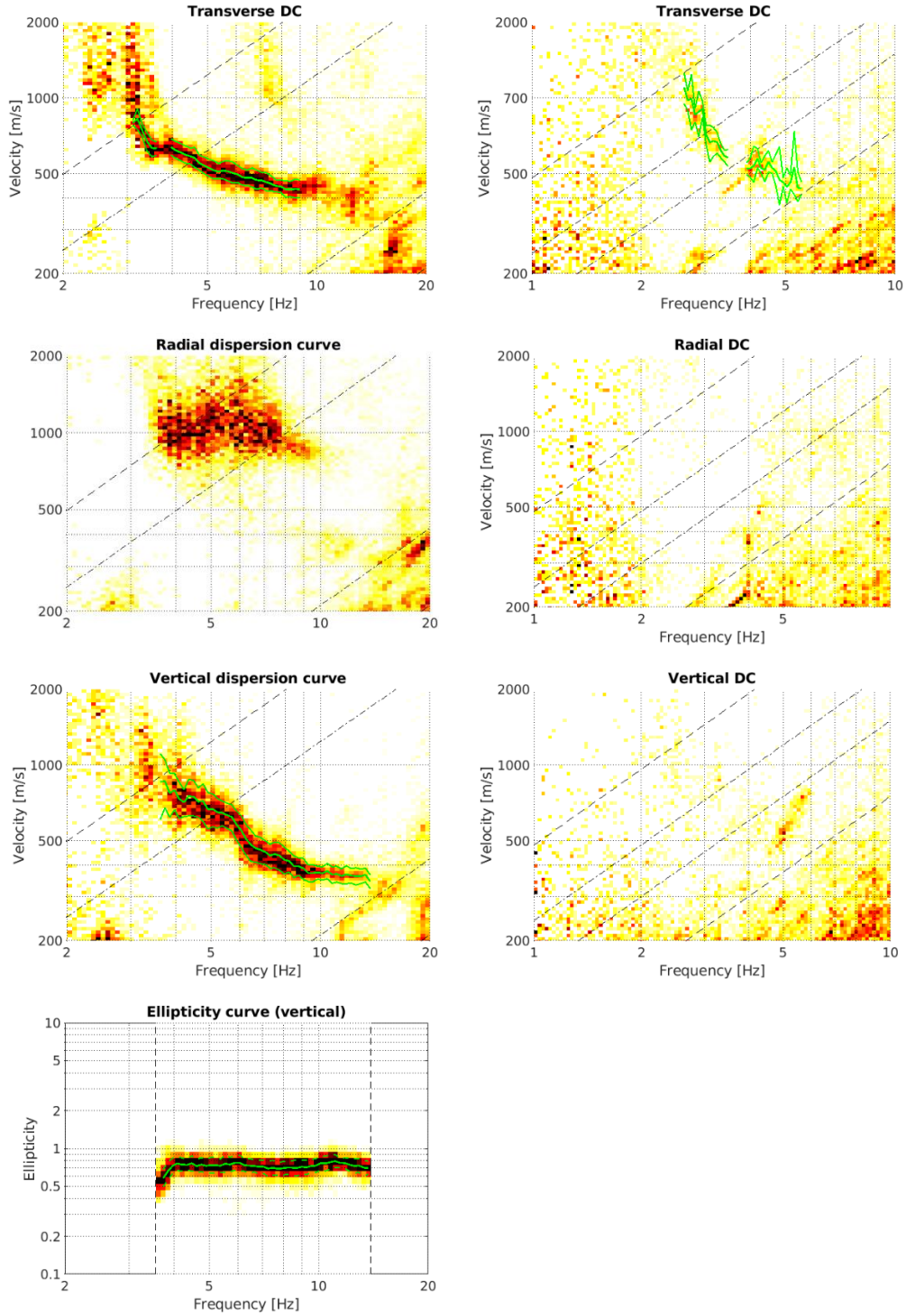


Figure 9: Dispersion and ellipticity curves for the transverse, radial and vertical components obtained with the 3-component HRFK algorithm (Poggi and Fäh, 2010) for configuration A (left column) and B (right column). The dashed and dotted black lines are the array resolution limits. The solid green lines are picked from the data, where the central line indicates the best value and the two outer lines the standard deviation.

### 3.5 WaveDec

The results of the WaveDec (Maranò et al., 2012) processing are shown in Fig. 10. This technique estimates the properties of single or multiple waves simultaneously with a maximum likelihood approach. In order to get good results, the parameter  $\gamma$  has been tuned to modify the sharpness of the wave property estimation between purely maximum likelihood estimation and a Bayesian Information Criterion. Here, a value of  $\gamma = 0.2$  was used, corresponding to a mostly maximum likelihood estimation.

A Love wave dispersion curve is clearly retrieved between 3.4 and 11.0 Hz. The Rayleigh wave dispersion curve can be picked between 4.0 Hz and 11.0 Hz. The ellipticity angle for the picked Rayleigh wave dispersion curve is positive below 5.0 Hz, indicating prograde particle motion, and negative above 5.0 Hz, indicating retrograde particle motion. This means that there is a singular trough at around 5.0 Hz, where the particle motion changes from prograde to retrograde.

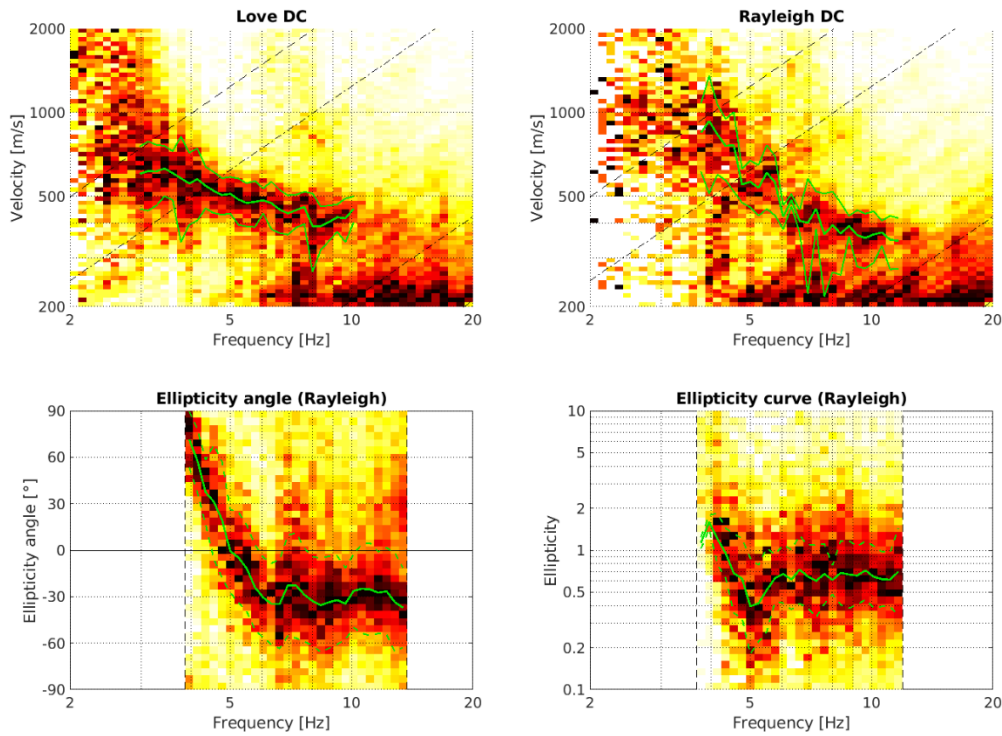


Figure 10: Dispersion and ellipticity curves for the Love and the Rayleigh waves obtained with WaveDec (Maranò et al., 2012). The dashed and dotted black lines are the array resolution limits. The solid green lines are picked from the data, where the central line indicates the best values and the two outer lines the standard deviation.

### 3.6 Summary

Fig. 11 gives an overview of the dispersion and ellipticity curves determined by the different methods. For Love waves, WaveDec gives a dispersion curve that is similar to HRFK. The phase velocities obtained using WaveDec and HRFK array B are slightly lower than those observed through HRFK array A. For the Rayleigh waves, there is also a good agreement between the two different methods.

The ellipticity curves retrieved using the different methods are quite similar. The RayDec curve seems shifted to lower frequencies compared with the WaveDec curve. The trough identified at 5.0 Hz with WaveDec is at around 4.0 Hz with RayDec. This is in agreement with the dipping interface hypothesis. As stations NAT49 and SNTZ are located on deeper sediments, their fundamental frequency is shifted to lower frequencies compared with the WaveDec curve, which was obtained for the array centered on shallower sediments. The change of particle motion seen by WaveDec indicates a singularity at the trough the curve. Therefore, we conclude that the ellipticity peak must also be a singularity and the particle motion of the fundamental mode is retrograde below and prograde above the peak frequency. The clear peak observed with RayDec at about 2.5 Hz should therefore be a singular peak.

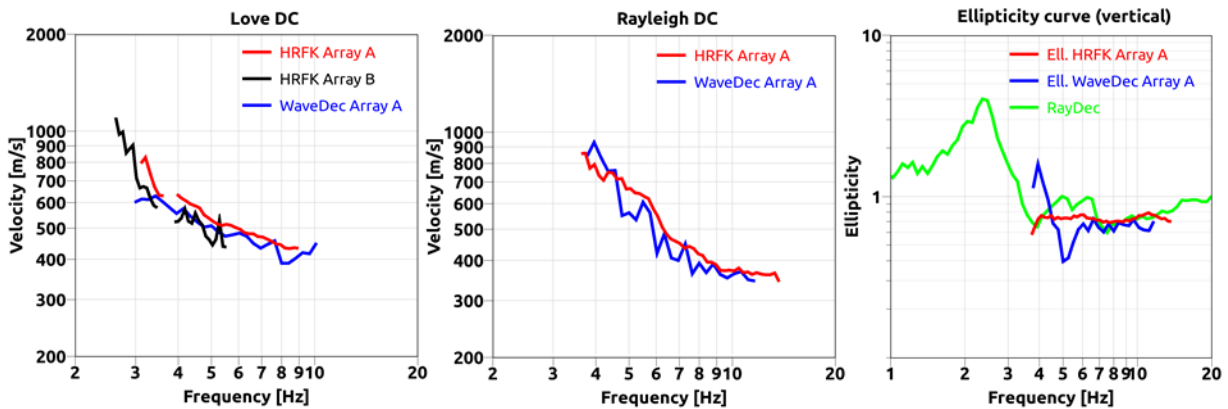


Figure 11: Comparison between the computed dispersion curves and ellipticity curves. The RayDec curve is related to the measurement point NAT49.

## 4 Data inversion

### 4.1 Inversion targets

We performed inversions using as much information as possible, using different parts of the picked dispersion and ellipticity curves. The details of these inversion targets are indicated in Table 1 and the corresponding curves are shown in Fig. 12.

In the first inversion, a combination of the HRFK curves obtained through Array A and B below 4.0 Hz was used as fundamental mode, whereas the curve of the HRFK array A above 4.0 Hz was used as first higher mode. For the Rayleigh waves, the curve obtained by HRFK for array A was considered as fundamental mode. As target for the Rayleigh wave ellipticity, we used the RayDec ellipticity curve of station NAT49, the measurement located nearby the strong motion station, around the fundamental peak. Only parts of the left and right flank of the peak were used

(Fig. 12), to constrain a singularity there. Using these information, we were unable to find velocity profiles explaining both the Rayleigh and Love dispersion curves.

A second inversion round, using all parts of the Love wave dispersion curves as fundamental mode, was then made. In this case, a good fit for Rayleigh and Love wave dispersion curves was achieved, but we didn't observe a singularity in the ellipticity (Fig. 13), even after forcing a strong velocity contrast at depth. The absence of this singularity can be a consequence of a too low velocity contrast at depth or the peak is not completely related to a 1D effect, but to possible 2D/3D effects, as might be visible in the polarization analysis. For this reason, the inversion was made by using only the Rayleigh and Love wave dispersion curves.

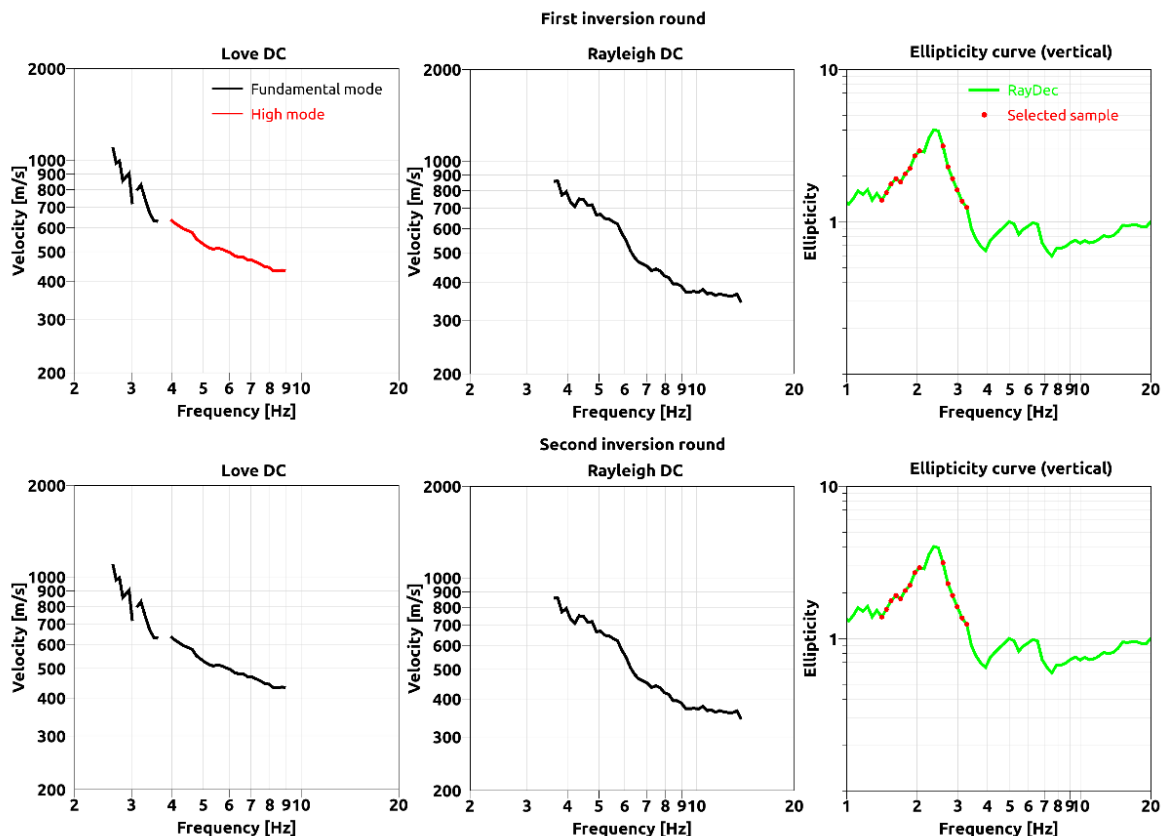


Figure 12: Overview of the dispersion curves used as targets for the different inversions.

Table 1: List of the data curves used as target in the inversion.

Method	Wave type	Mode	Curve type	Frequency range [Hz]
HRFK (T)	Love	fundamental	dispersion	2.6-9.0
HRFK (T)	Rayleigh	fundamental	dispersion	3.6-14.0
RayDec (NAT49)	Rayleigh	fundamental	ellipticity	1.4-2.0
RayDec (NAT49)	Rayleigh	fundamental	ellipticity	2.5-3.3

## 4.2 Inversion parameterization

For the inversion, six different parameterizations are used in total. The first five have free values of the depths and velocities of the different layers, ranging from four to eight layers (including half-space). The last parameterization has fixed layer depths and consists of 15 layers in total, with the deepest interface at 70m depth.

The S- and P-wave velocities are allowed to range from 150 to 1500 m/s and from 200 to 5000 m/s, respectively. The deepest layer interfaces were allowed to range to a depth of 150 m for all parameterizations. The density was fixed to 2300 kg/m<sup>3</sup> for the bedrock layer and to 2000 kg/m<sup>3</sup> for all other layers.

## 4.3 Inversion results

We performed a total of seven inversions with different parameterizations (see Table 2). Each inversion run produced 200000 total models in order to assure a good convergence of the solution. The results of these inversions are shown in Figs 13 – 19.

The inversion SNTZ7le is shown as best example result of the second inversion round, to highlight the impossibility to fit a singularity on the ellipticity curve.

The remaining inversions results, from SNTZ4l to SNTZfix, fit the data comparably well and give similar minimum misfit values.

*Table 2: List of inversions*

Inversion	Number of layers	Number of models	Minimum misfit
SNTZ7le	7	200000	0.377
SNTZ4l	4	200000	0.416
SNTZ5l	5	200000	0.406
SNTZ6l	6	200000	0.421
SNTZ7l	7	200000	0.395
SNTZ8l	8	200000	0.428
SNTZfix	15	200000	0.398

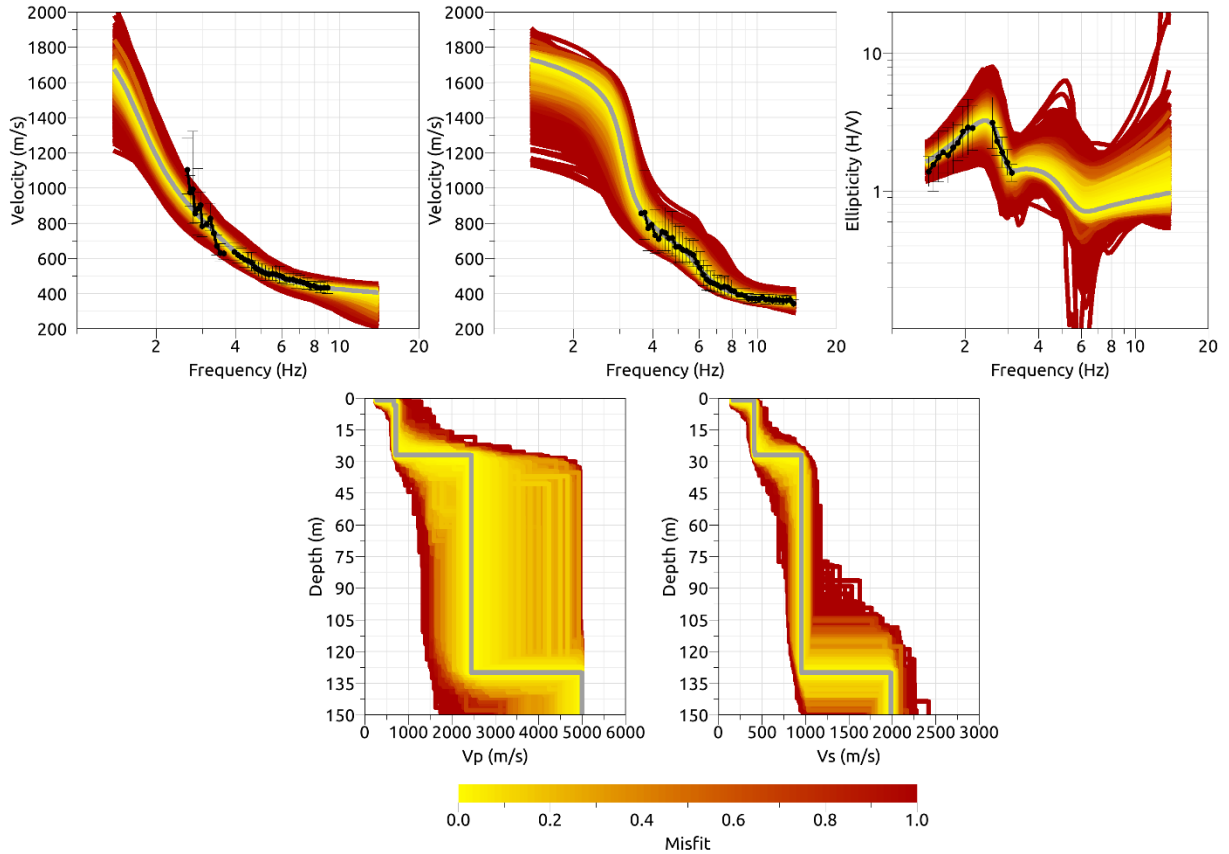


Figure 13: Inversion SNTZ7le. Top line: Dispersion curves for the Love wave fundamental mode (left) and the Rayleigh wave fundamental mode (center), ellipticity curve of the Rayleigh wave fundamental mode (right). Bottom line: P-wave velocity profiles (left) and S-wave velocity profiles (right). The black dots indicate the data points used for the inversion, the gray line indicates the best-fitting model.

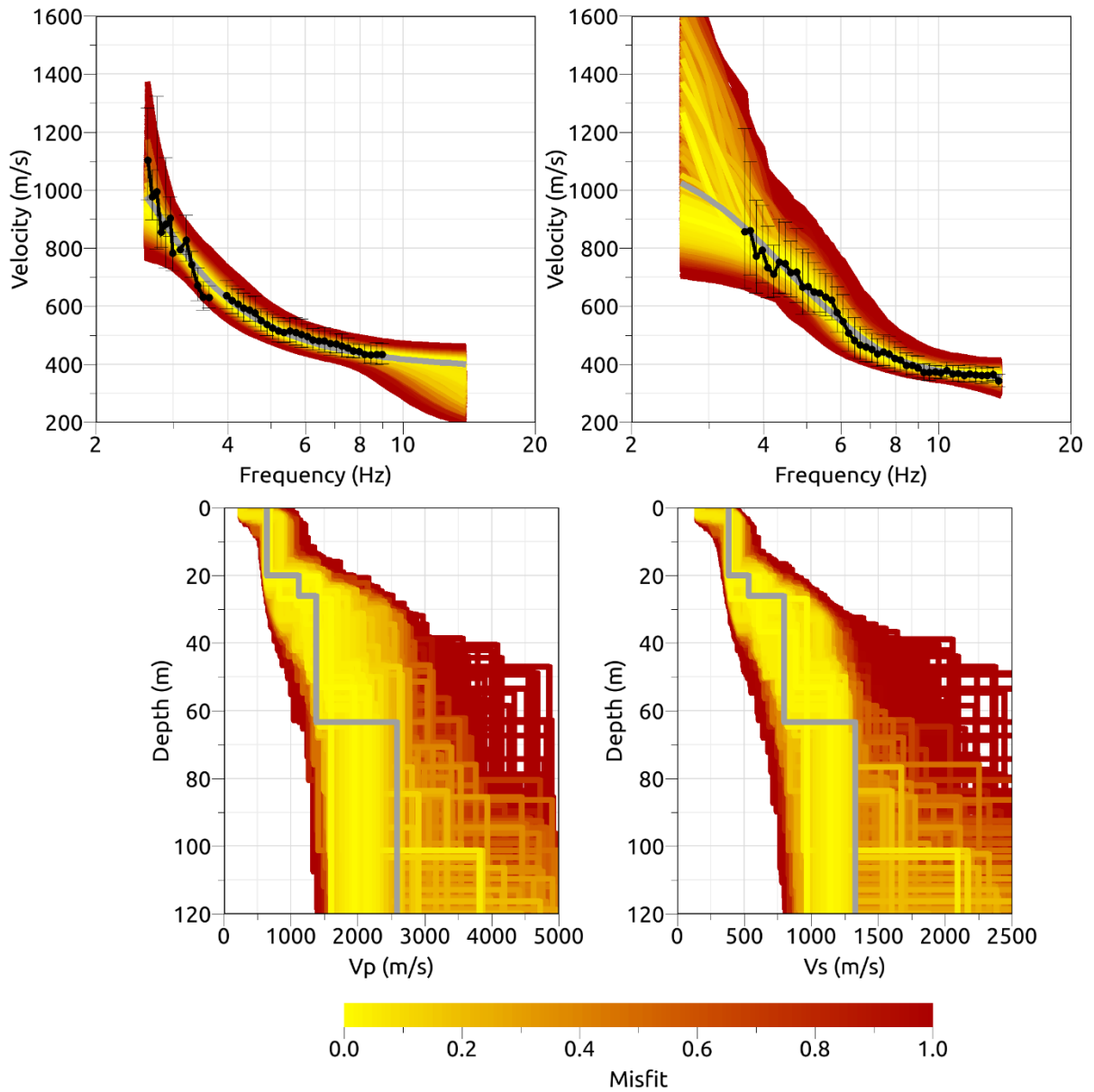


Figure 14: Inversion SNTZ41. Top line: Dispersion curves for the Love wave fundamental mode (left) and the Rayleigh wave fundamental mode (right). Bottom line: P-wave velocity profiles (left) and S-wave velocity profiles (right). The black dots indicate the data points used for the inversion, the gray line indicates the best-fitting model.

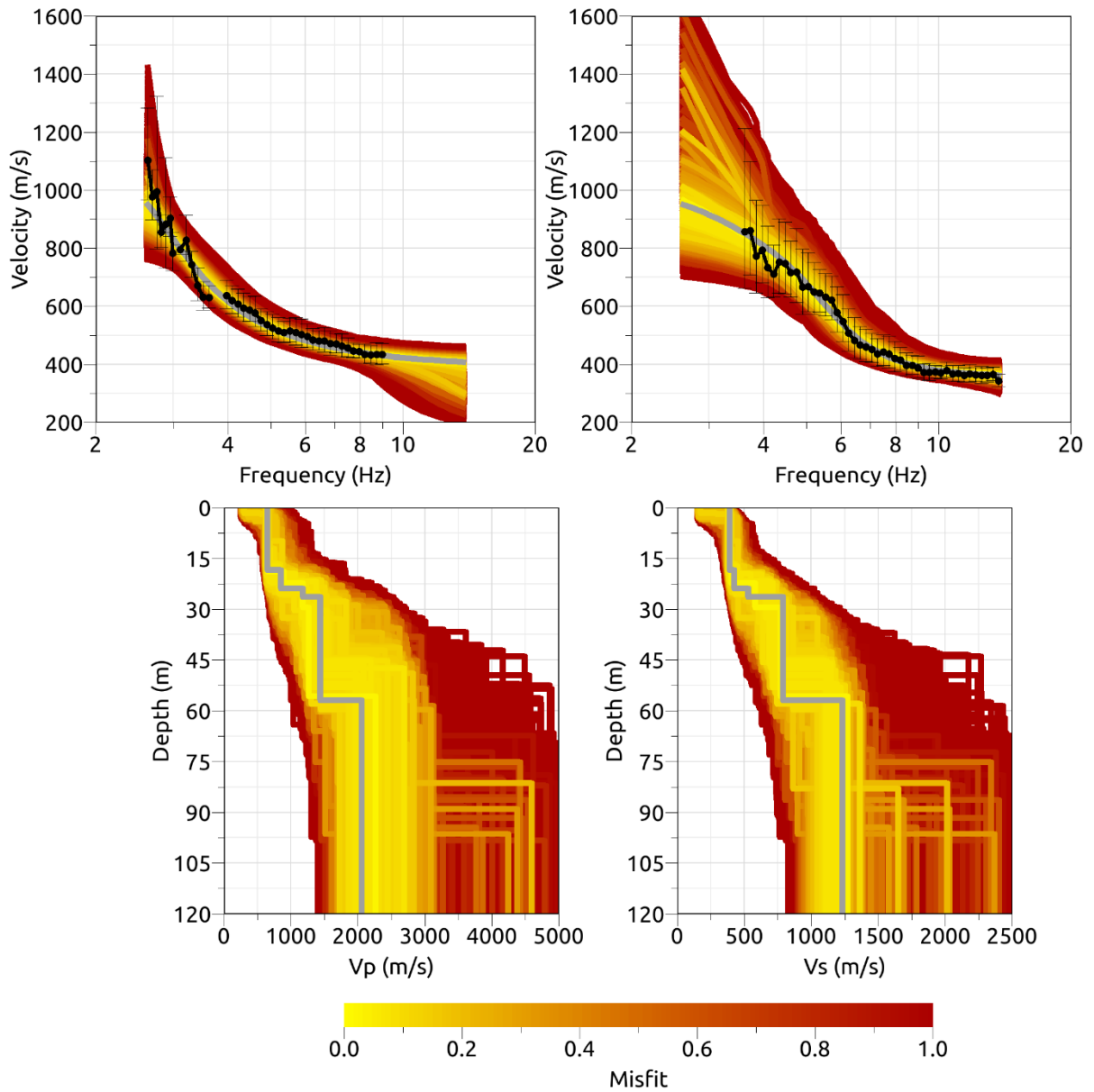


Figure 15: Inversion SNTZ5l. Top line: Dispersion curves for the Love wave fundamental mode (left) and the Rayleigh wave fundamental mode (right). Bottom line: P-wave velocity profiles (left) and S-wave velocity profiles (right). The black dots indicate the data points used for the inversion, the gray line indicates the best-fitting model.

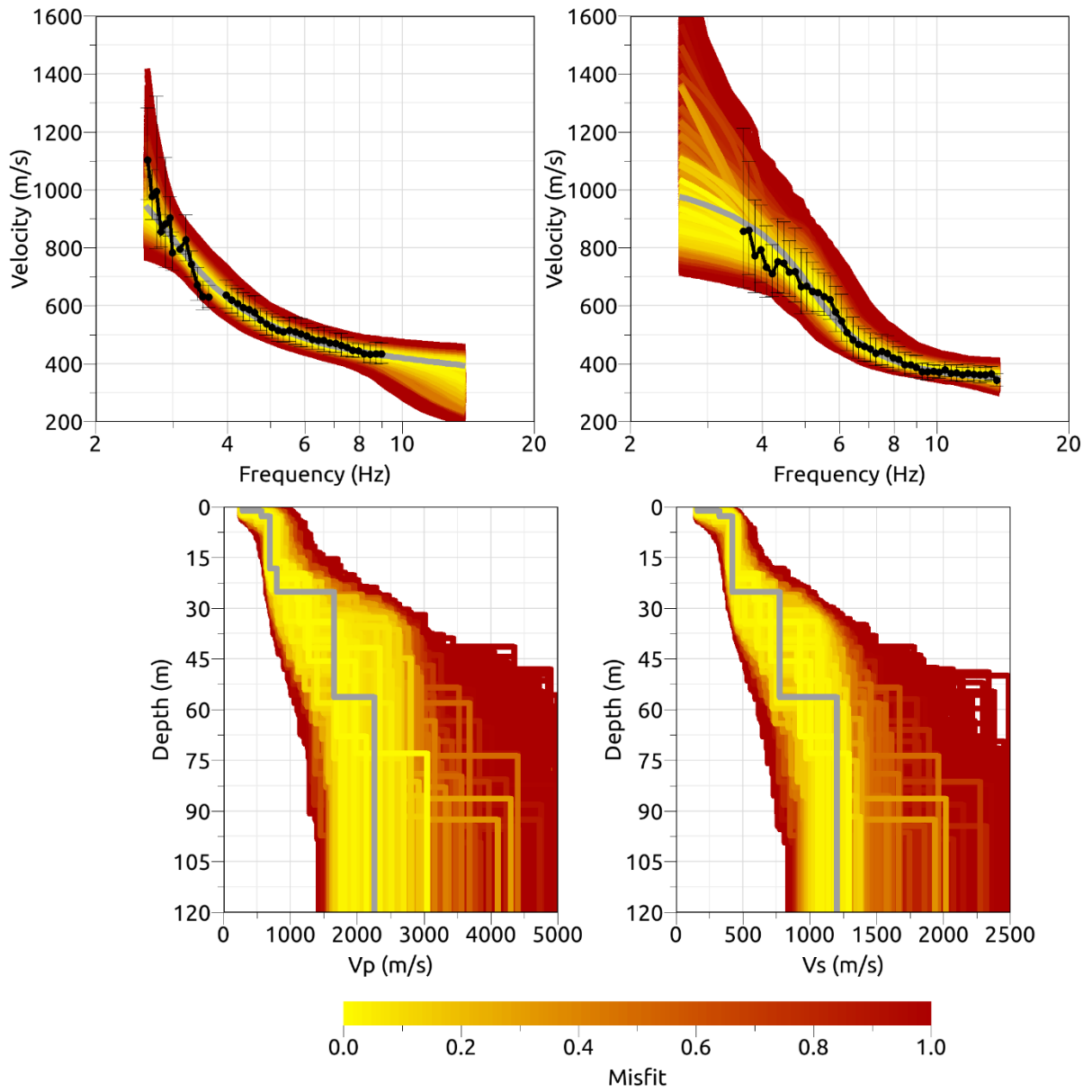


Figure 16: Inversion SNTZ6l. Top line: Dispersion curves for the Love wave fundamental mode (left) and the Rayleigh wave fundamental mode (right). Bottom line: P-wave velocity profiles (left) and S-wave velocity profiles (right). The black dots indicate the data points used for the inversion, the gray line indicates the best-fitting model.

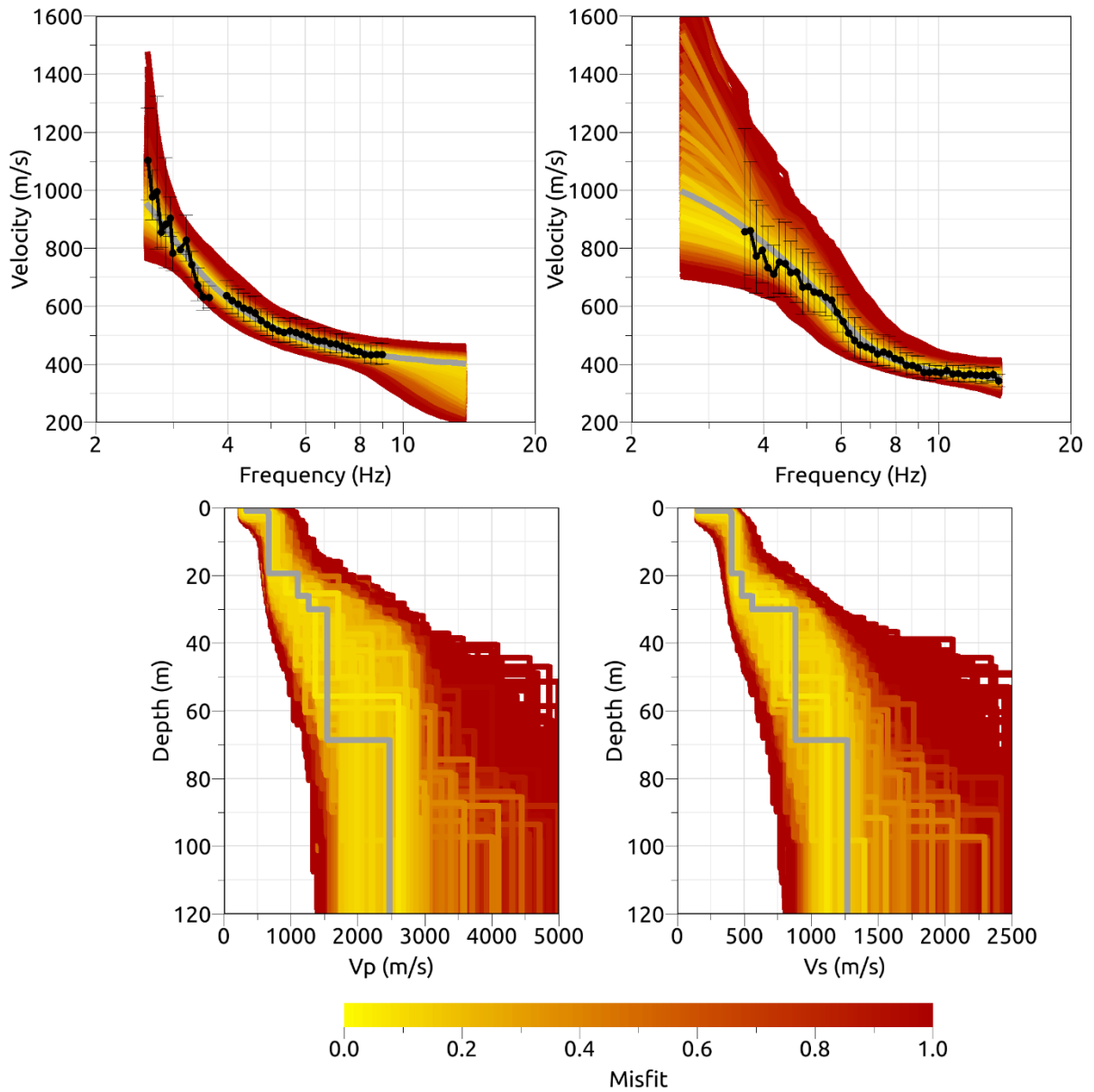


Figure 17: Inversion SNTZ7L. Top line: Dispersion curves for the Love wave fundamental mode (left) and the Rayleigh wave fundamental mode (right). Bottom line: P-wave velocity profiles (left) and S-wave velocity profiles (right). The black dots indicate the data points used for the inversion, the gray line indicates the best-fitting model.

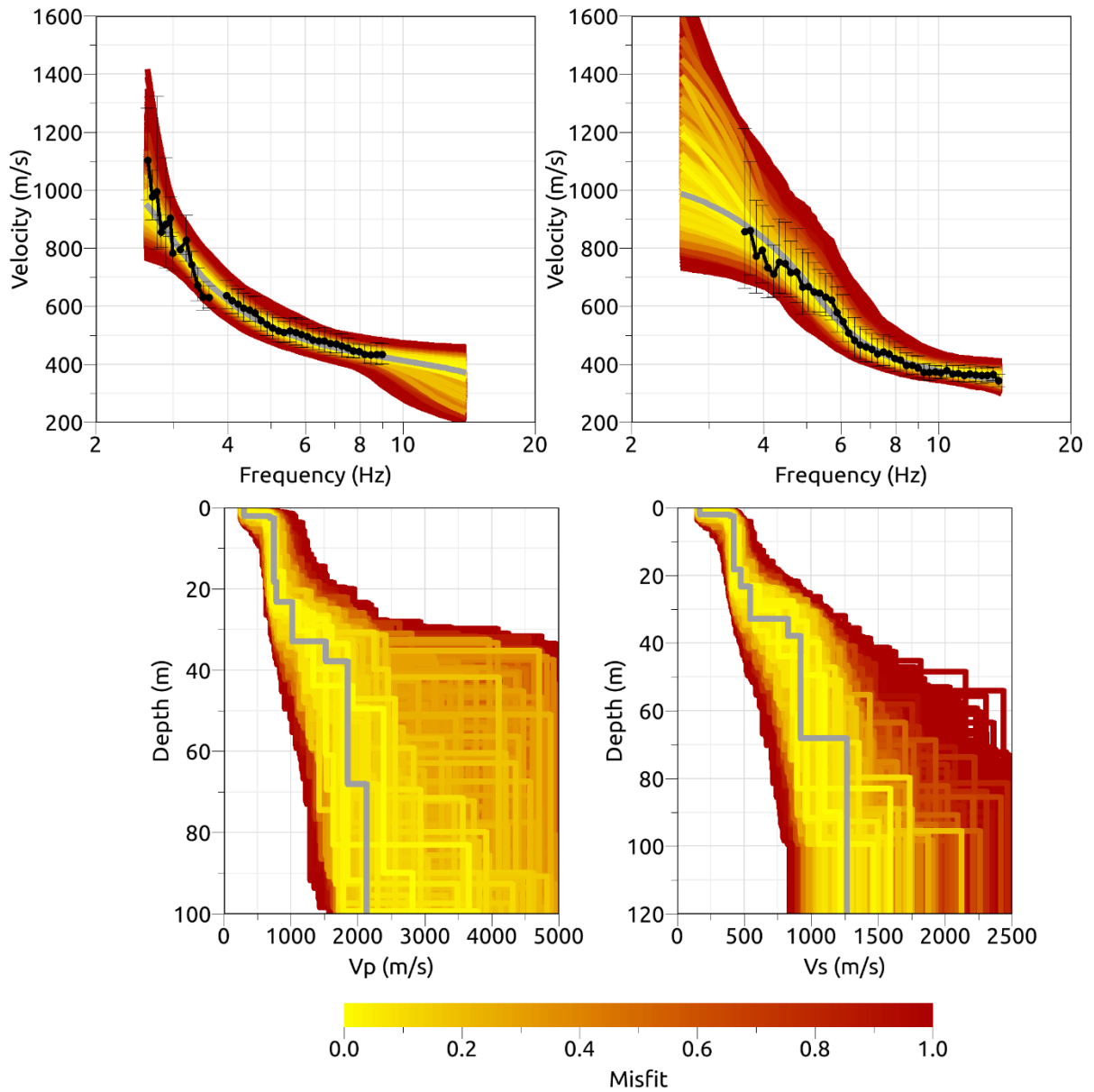


Figure 18: Inversion SNTZ81. Top line: Dispersion curves for the Love wave fundamental mode (left) and the Rayleigh wave fundamental mode (right). Bottom line: P-wave velocity profiles (left) and S-wave velocity profiles (right). The black dots indicate the data points used for the inversion, the gray line indicates the best-fitting model.

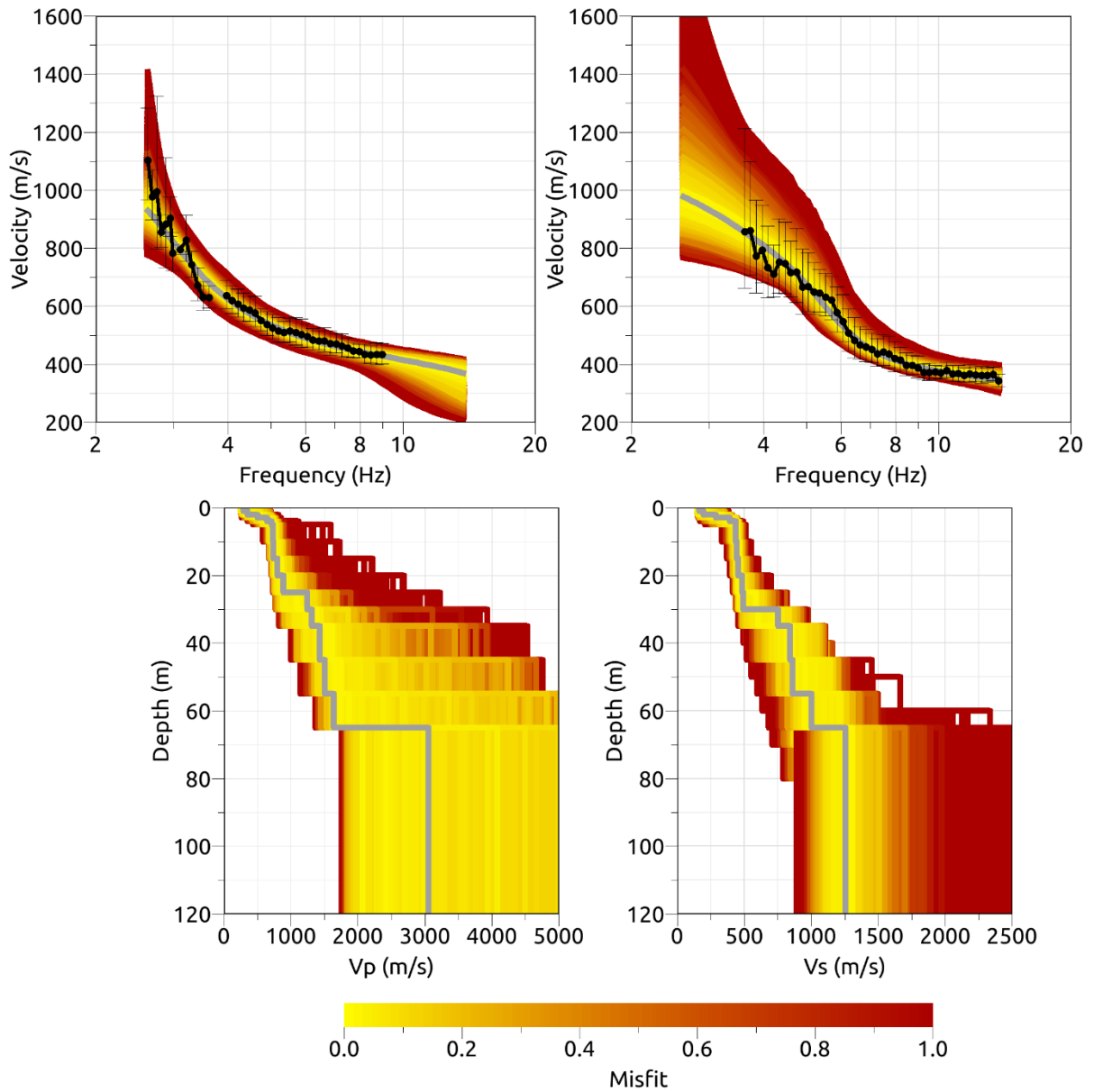


Figure 19: Inversion SNTZfix. Top line: Dispersion curves for the Love wave fundamental mode (left) and the Rayleigh wave fundamental mode (right). Bottom line: P-wave velocity profiles (left) and S-wave velocity profiles (right). The black dots indicate the data points used for the inversion, the gray line indicates the best-fitting model.

#### 4.4 Discussion of the inversion result

The best-fitting models of the inversions are shown in Fig. 20. There are several main characteristics that all models have in common. The seismic bedrock is found at depths between 56.0 and 73.0 m, with a shear wave velocity of about 1200 m/s. The bedrock depth probably has a slight variability in depth because no ellipticity was used in the inversion and the bedrock is dipping below the seismic stations of the array. Above the bedrock, the S-wave velocity is about 850.0 m/s up to a depth of 25.0 to 32.0 m. The S-wave velocity decreases then to about 420 m/s up to 2.0 m of depth. In the upper 2.0 m, the velocity profiles show a low velocity with S-wave of about 200 m/s.

The velocity profiles resulting from the different inversions have  $V_{S30}$  between 405.8 and 437.1 m/s, with an average value of  $418.4 \pm 12.5$  m/s.

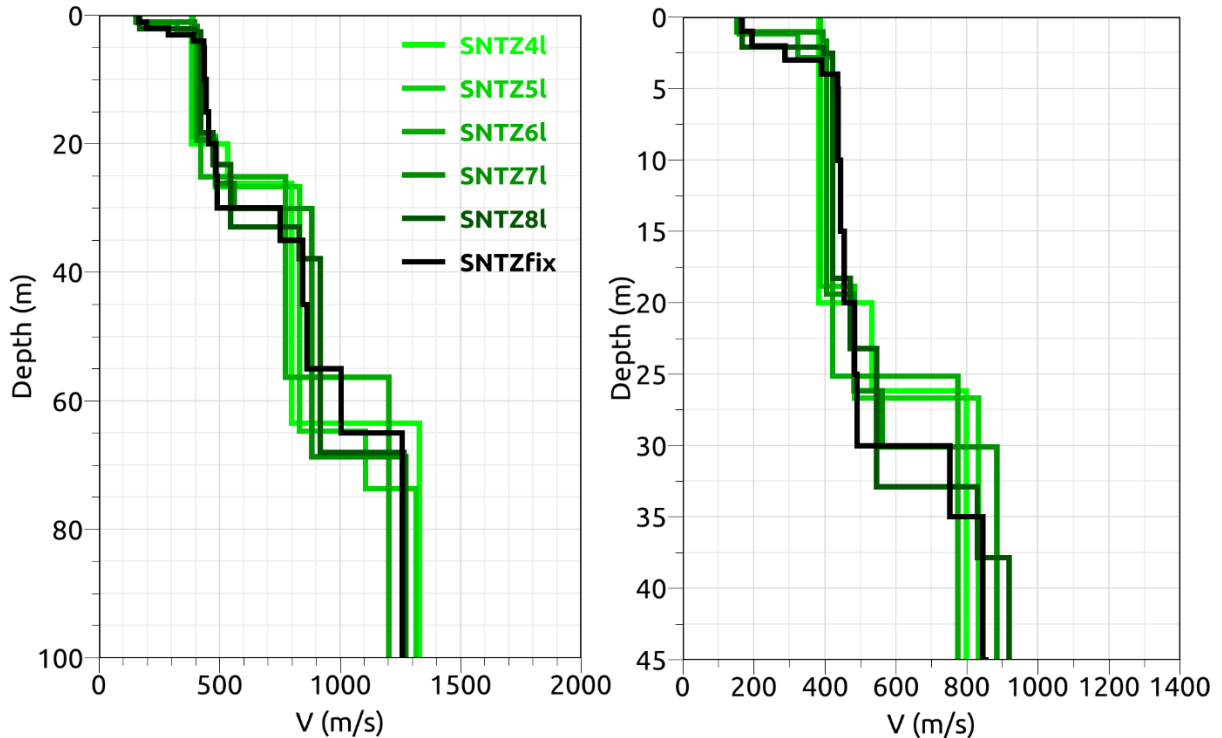


Figure 20: Overview of the shear-wave velocity profiles of the different inversions (left) and zoom on the upper 35 m of the inversion profiles.

## 5 Further results from the inverted profiles

### 5.1 SH transfer function

In Fig. 21, the theoretical shear-wave transfer functions for the inverted models are shown. In this case, the models are predicting an amplification up to a factor of 3 at about 3.0 Hz. This will be compared to observations of earthquake recordings at this station in the future, as soon as the station has recorded a sufficiently large number of earthquakes.

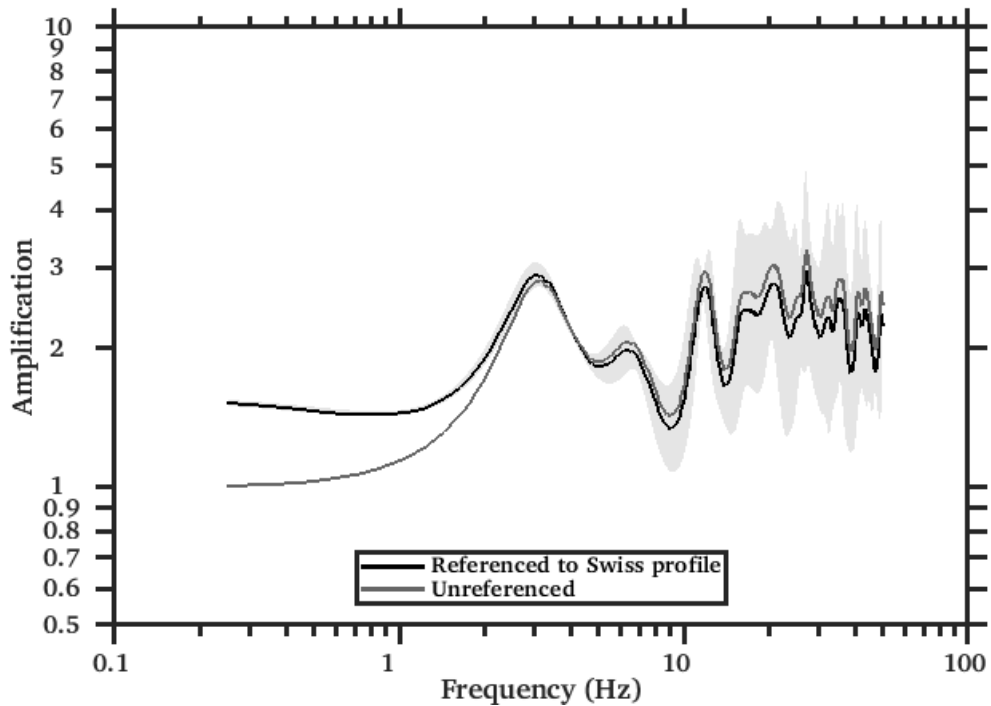


Figure 21: Modeled amplification function for the best models of the six inversions.

## 5.2 Quarter-wavelength representation

The quarter-wavelength velocity approach (Joyner et al., 1981) provides, for a given frequency, the average velocity at a depth corresponding to 1/4 of the wavelength of interest (Fig. 22). The results using this proxy, considering frequency limits of the experimental data of 2.0 to 2.5 Hz for the dispersion curves, is well constrained above 100 m. The quarter wavelength impedance-contrast introduced by Poggi et al. (2012) is also displayed in the figure. It corresponds to the ratio between two quarter-wavelength average velocities, respectively from the top and the bottom part of the velocity profile, at a given frequency.

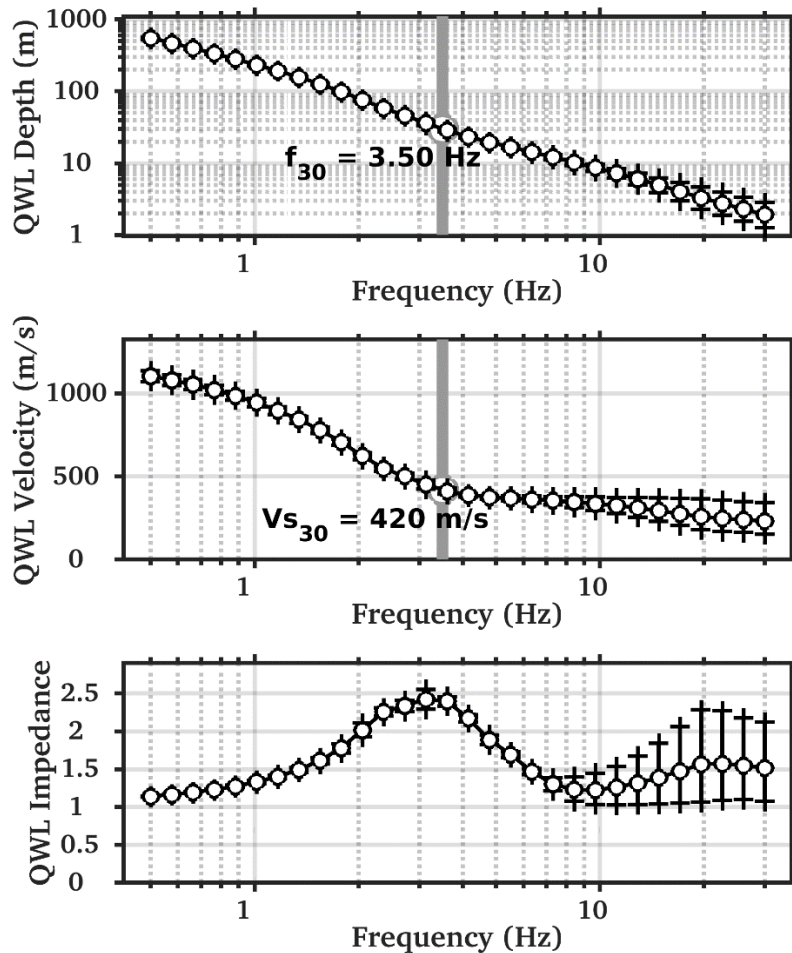


Figure 22: Quarter wavelength representation of the velocity profiles for the best models of the inversions (top: depth, center: velocity, bottom: inverse of the impedance contrast). The grey bar corresponds to  $f_{30}$  (frequency related to the of 30 m) and  $V_{s30}$ .

## 6 Discussion and conclusions

The H/V analysis points out that the fundamental peak observed at the different stations is variable and can be explained by a dipping bedrock towards SE.

The inversion of the passive seismic array measurements yields a velocity profile with 3 main interfaces at about 5, 30 and 70 m. In particular, the last one corresponds to the bedrock having a velocity of about 1200 m/s. Above the bedrock,  $V_S$  ranges between 200 m/s at the surface and 850 m/s at depth. The  $V_{S30}$  value of the site is determined as about 418 m/s, corresponding to soil class B in EC8 and C in SIA261 classifications. The  $V_{S30}$  may appear high for this site located on alluvial deposits, but it is important to remember the results of polarization analysis in the site NAT49, that highlights a possible 2D/3D behavior of the alluvial fan.

The theoretical shear-wave transfer function predicts an amplification factor of around 3 at about 3.0 Hz, in quite good agreement with the 2.5 Hz fundamental frequency of the site where the strong motion station is installed. This will be compared to observations at this station in the future.

## References

- Burjánek, J., Gassner-Stamm, G., Poggi, V., Moore, J. R., and Fäh, D. (2010). Ambient vibration analysis of an unstable mountain slope. *Geophys. J. Int.*, 180:820–828.
- Burjánek, J., Moore, J. R., Molina, F. X. Y., and Fäh, D. (2012). Instrumental evidence of normal mode rock slope vibration. *Geophys. J. Int.*, 188:559–569.
- Fäh, D., Gardini, D., et al. (2003). Earthquake Catalogue of Switzerland (ECOS) and the related macroseismic database. *Eclogae geol. Helv.* 96.
- Fäh, D., Wathelet, M., Kristekova, M., Havenith, H., Endrun, B., Stamm, G., Poggi, V., Burjanek, J., and Cornou, C. (2009). Using ellipticity information for site characterisation. NERIES deliverable JRA4 D4, available at <http://www.neries-eu.org>.
- Fritsche, S., Fäh, D., Gisler, M., and Giardini, D. (2006). Reconstructing the damage field of the 1855 earthquake in Switzerland: historical investigations on a well-documented event *Geophys. J. Int.*(2006)166,719–731
- Hobiger, M., Bard, P.-Y., Cornou, C., and Le Bihan, N. (2009). Single station determination of Rayleigh wave ellipticity by using the random decrement technique (RayDec). *Geophys. Res. Lett.*, 36.
- Maranò, S., Reller, C., Loeliger, H.-A., and Fäh, D. (2012). Seismic waves estimation and wavefield decomposition: Application to ambient vibrations. *Geophys. J. Int.*, 191:175–188.
- Panzer, F., D'Amico, S., Lupi, M., Mauri, G., Karyono, K., and Mazzini, A. (2018). Lusi hydrothermal structure inferred through ambient vibration measurements. *Marine and Petroleum Geology* 90, 116-124
- Poggi, V. and Fäh, D. (2010). Estimating Rayleigh wave particle motion from three component array analysis of ambient vibrations. *Geophys. J. Int.*, 180:251–267.

Poggi, V., Edwards, B., and Fäh, D. (2010). Characterizing the Vertical-to-Horizontal Ratio of Ground Motion at Soft-Sediment Sites. *Bulletin of the Seismological Society of America*, 102(6): 2741-2756.